Effects of Metal Ion Binding on Structural Dynamics of Human Hemopexin†

Federico I. Rosell, Marcia R. Mauk, and A. Grant Mauk*

Department of Biochemistry and Molecular Biology and Centre for Blood Research, University of British Columbia, Vancouver, British Columbia V6T 1Z3, Canada

Received April 27, 2007; Revised Manuscript Received May 31, 2007

ABSTRACT: Hemopexin (Hx) functions as a major heme scavenging protein in blood plasma and as such circulates without heme bound. In recent work, we have demonstrated that Hx binds metal ions in vitro in a manner that varies from one metal ion to another and that changes with heme binding. The structural consequences of metal ion binding to the form of Hx that dominates in plasma have now been evaluated by monitoring metal ion-linked changes in tertiary structure of the protein as reflected by changes in the near-UV CD spectrum and the ultraviolet absorption spectrum as a function of temperature. As part of this analysis we have developed thermally induced difference absorption maps (TIDAMs) to afford efficient visualization of temperature-dependent changes in the UV spectrum of Hx that are induced by binding of metal ions. The results are interpreted in terms of recent models proposed for metal ion binding sites on Hx and have implications for the possible modulation of heme binding to Hx by metal ions in vivo.

Hemopexin (Hx)[1] (MW ∼58000) is a type II acute phase reactant glycoprotein that scavenges heme in blood plasma to protect against oxidative damage (*1*−*3*) resulting from the catalytic activity of heme released to the circulation by hemolysis or rhabdomyolysis (*4*−*6*). The Hx−heme complex is rapidly removed from circulation predominantly by hepatocytes through receptor-mediated mechanisms (*7*−*10*). Receptor-mediated uptake of the Hx−heme complex leads either to encapsulation of the complex in endosomes, a fate compatible with the return of Hx to the circulation (*11*) following release of heme, or in lysosomes, a fate leading to proteolysis with no return of Hx to the circulation (*8*).

Following an initial report of the three-dimensional structure for the C-domain of rabbit Hx (*12*), Paoli et al. reported the crystal structure of the full-length rabbit Hx−heme complex (*13*). In that structure, a single heme is bound between the N- (residues 1−208) and C- (residues 228−435) domains by two histidyl residues. One of these heme axial ligands (His266) is located in the C-domain, and the other (His213) is located in the flexible hinge region that links the two domains. The human and rabbit proteins are expected to exhibit considerable structural similarity based on ∼80% sequence identity. Homology modeling has been used recently (*14*) to produce a structural model for the human protein that diverges from that of the rabbit protein in just two regions. The first of these regions is located in the linker sequence that connects the two major structural domains. This sequence is four residues longer in the human protein and contains an additional His residue as well as an additional site of glycosylation. The second region of divergence is in a loop of the N-domain around residue 100. This region comprises a site at which the human Hx−heme complex is susceptible to hydrolysis by trypsin and plasmin but the rabbit complex is not (*15*).

Binding of metal ions, particularly Zn^{2+} or Cu^{2+}, to the human Hx−heme complex reduces the thermal stability of the complex (*16*), providing a potential mechanism for heme release in hepatic endosomes. Several putative metal ion binding sites have been identified in the model of the human Hx−heme complex (*14*). While the principal form of Hx in plasma does not contain heme, it does have the ability to bind a variety of metal ions as reviewed recently (*14*), and consequently, Hx may play a role in plasma metal ion homeostasis. Accordingly, binding of metal ions to Hx is expected to influence the heme-scavenging activity of the protein, possibly through the alteration of protein structure. To consider this possibility further, the effects of metal ions on the structure of the circulating form of Hx have now been studied by ultraviolet electronic and circular dichroism spectroscopies.

MATERIALS AND METHODS

Sample Preparation. Human Hx was prepared from frozen samples of the cryosupernatant fraction of human plasma as described previously (*17*). However, following elution from the Ni^{2+}-HiTrap column, Hx was exchanged into sodium phosphate buffer [50 mM containing 150 mM NaCl (pH 7.4)], and trace amounts of a high molecular weight contaminant were removed with a Superdex 75 (10/300 GL) (Amersham Bioscience) column. Following addition of EDTA (final concentration 10 mM, pH 7.4), the Hx was exchanged into one of three working buffers [(i) sodium phosphate buffer (10 mM, pH 7.4), (ii) PBS (10 mM sodium

†This work was supported by a Canadian Blood Services−Canadian Institute of Health Partnership Grant and a Canada Research Chair (A.G.M.). The spectropolarimeter and spectrophotometer were funded by grants from the Canadian Foundation for Innovation to the UBC Laboratory of Molecular Biophysics and the Centre for Blood Research and operated with support of the Michael Smith Foundation for Health Research.

* Author to whom correspondence should be addressed. Telephone: (604)822-3719. Fax: (604)822-6860. E-mail: mauk@interchange.ubc.ca.

[1] Abbreviations: Hx, hemopexin; heme, iron protoporphyrin IX; PBS, phosphate-buffered saline; TIDAM, thermally induced difference absorption map; GdnHCl, guanidine hydrochloride.

10.1021/bi7008079 CCC: $37.00
Published on Web 07/18/2007

phosphate buffer, 2.7 mM KCl, and 137 mM NaCl, pH 7.4), or (iii) bisTris-HCl buffer (50 mM containing 50 mM NaCl, pH 5.0)] by centrifugal ultrafiltration (Amicon Ultra 30000 NMWL). The concentration of Hx was determined from the molar absorptivity at 280 nm of 123000 M^{-1} cm^{-1} (*17*).

For all thermal dependence studies, a protein concentration of 5 μM was used. In experiments involving metal ions, $ZnCl_2$, $CoCl_2$, $CuCl_2$, $MnCl_2$ (Titrisol standards; EM Science), or $NiCl_2$ (hexahydrate salt; Sigma) was added 20 min before initiating the thermal ramp. A final metal ion concentration of 100 μM was selected to saturate the principal metal ion binding site(s) of the protein as judged from previous potentiometric titrations (*17*). These protein and metal ion concentrations are the same as those used previously to assess the effect of metal ion binding on the stability of the Hx−heme complex (*16*), thereby facilitating comparison of results. To measure electronic absorption spectra, the protein solution (0.8 mL) was placed into a masked 1 cm path length semi-micro quartz cuvette and overlaid with light mineral oil (0.4 mL) before the cell was sealed with a Teflon stopper. For far-UV CD measurements, the protein sample (0.4 mL) was placed into a rectangular quartz cuvette (1 mm path length) and sealed with a Teflon stopper. GdnHCl solutions were prepared from material recrystallized according to the method of Nozaki (*18*) or Ultrapure grade from Invitrogen.

Temperature-Dependent Spectroscopic Measurements. The thermal dependence of Hx electronic spectra in the presence and absence of metal ions was monitored spectrophotometrically with a Cary 6000i spectrophotometer equipped with a Peltier device for temperature control. Spectra (255−310 nm) were collected at 2.5 °C intervals between 10 and 90 °C with a 1 nm spectral bandwidth, 0.04 nm data interval, and 0.1 s averaging time. Thermal dependence was also monitored by CD spectroscopy with a Jasco J-810 spectropolarimeter fitted with a Peltier device. The ellipticity at 231 nm, which is regarded generally as a sensitive indicator of the integrity of the tertiary structure of Hx (*13*, *19*−*21*), was recorded as a function of temperature (2 nm bandwidth, 1 s response time) at 0.1 °C intervals from 3 to 95 °C. For simplicity, the ellipticity at 231 nm is referred to subsequently as CD_{231}. The average temperature gradient in all experiments was 1.0−1.2 °C/min, and the Peltier devices in both spectrometers were calibrated as described previously (*16*).

Data Analysis. All electronic absorption spectra were corrected for the temperature-dependent changes in solvent volume as described by Demchenko (*22*). The solution densities were estimated to be the sum of the density increments calculated for each component using parameters and equations reported by Laue et al. (*23*). Second and fourth derivative spectra were produced with GRAMS/AI (v. 7.00; ThermoGalactic) using a λ-shift of 1.6 nm as described by Butler (*24*) and Lange et al. (*25*). A 27-point Savitsky−Golay smoothing function was applied to the final derivative spectrum.

The degree of tryptophan exposure in Hx and complexes it forms with metal ions was estimated at 20 °C according to the method of Shevchenko et al. (*26*) prior to initiating thermal ramps. The average Tyr exposure (*r*) in Hx and its metal complexes was determined as a function of temperature from the second derivative absorption spectra according to Ragone et al. (*27*) and subsequent reviews (*28*, *29*). The intensities of the peak maxima (∼287 and 295 nm) and trough minima (∼283 and 291 nm) were used in this calculation. The temperature dependence of *r* and the corresponding CD_{231} monitored for each sample were fitted by nonlinear least-squares analysis to a two-state model (Scientist v. 2.01; Micromath) as described previously (*16*) to obtain the transition midpoint temperature (T_m), the enthalpy change (ΔH_m), and the change in heat capacity (ΔC_p).

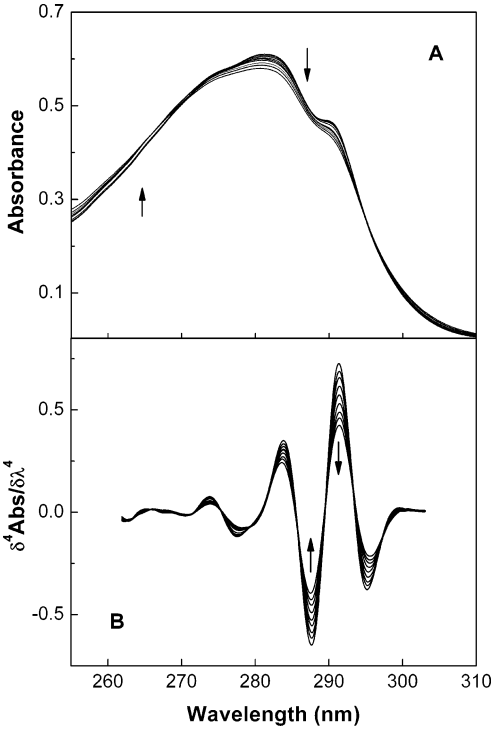

FIGURE 1: Temperature dependence of the near-UV spectrum of Hx in sodium phosphate buffer (10 mM, pH 7.4). Spectra are shown at 10 °C intervals between 10 and 90 °C. The arrows indicate the direction of spectral change with increasing temperature. (A) Electronic absorption spectra at 10 °C intervals between 10 and 90 °C prior to correction for the change in solution density with temperature. (B) Fourth derivative absorption spectra. The derivative spectra were produced from baseline and density-corrected absorption spectra using successive 1.60, 1.55, 1.63, and 1.60 nm shifts and a final smoothing by the method of Savitsky and Golay.

Thermally induced difference absorption maps (TIDAMs) were constructed from the density-corrected UV absorption spectra using a 2.5 °C perturbation step. The convention of lower minus higher temperature spectrum was applied, and the resulting difference spectrum was assigned to the average of the two temperatures. The contour and 3D surface plots in which the three axes represent wavelength, temperature, and absorbance difference were prepared with the program Origin (v. 7.5; OriginLab Corp.). The same procedure was applied to the fourth derivative absorption spectra computed with GRAMS/AI to generate difference contour plots in which the *z*-axis represents the change in fourth derivative intensity.

RESULTS

Thermal Dependence of Human Hx Ultraviolet Spectroscopic Properties. On heating Hx from 10 to 90 °C, the UV absorption spectrum exhibits a slight blue shift and decreases in intensity (Figure 1A). Calculation of the second (not

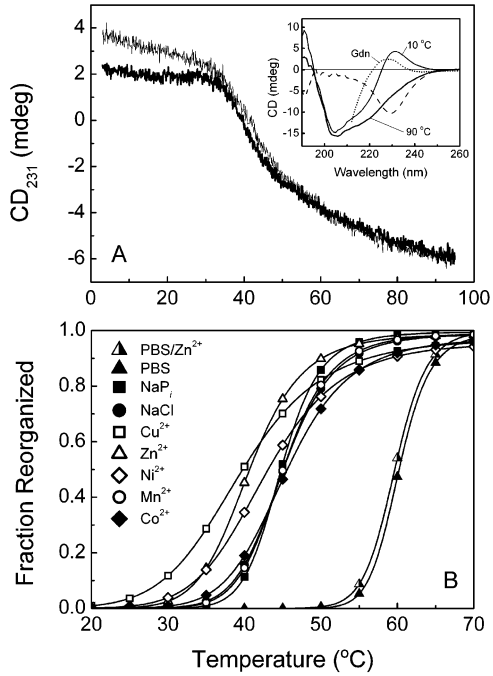

FIGURE 2: Thermal reorganization of Hx and of complexes formed by Hx with metal ions in sodium phosphate buffer (10 mM, pH 7.4) as monitored by far-UV CD spectroscopy. (A) Effect of temperature on the ellipticity at 231 nm of complexes formed by Hx with Zn^{2+} (bold line) or Ni^{2+} (light line). The inset shows the CD spectrum of Hx at 10 °C and at 90 °C, the calculated difference spectrum (dashed line), and the partial CD spectrum of the protein in the same buffer with 6 M GdnHCl at 10 °C (dotted line). (B) Temperature dependence for reorganization of Hx (5 μM) in sodium phosphate buffer (10 mM, pH 7.4) (■), supplemented with 100 μM $CuCl_2$ (□), $NiCl_2$ (◇), $ZnCl_2$ (△), $CoCl_2$ (◆), $MnCl_2$ (○), or 200 μM NaCl (●), and in PBS (▲) with 100 μM $ZnCl_2$ (▲). Equations 1−3 of ref *16* were used to fit the data. Parameters from these fits were used to calculate the lines shown.

shown) and fourth derivatives (Figure 1B) of the absorption spectrum allows resolution of the small spectroscopic shifts of the component aromatic residue absorption bands while minimizing contributions from light scattering. The fourth derivative spectrum exhibits multiple isosbestic points (275.6, 279.2, 286.5, 290.0, and 293.8 nm) as well as a complex pattern of band shifts with increasing temperature that are difficult to appreciate in the standard presentation format (Figure 1B). For example, the maximum at ~283 nm shifts to shorter wavelength with increasing temperature while the maximum at ~291 nm shifts initially to longer wavelength before reversing direction at higher temperatures. The minimum at 287 nm shifts to the blue at more elevated temperatures, and the minimum at ~295 nm shifts to the red in a nearly monotonic manner throughout the thermal gradient. The major change in the near-UV CD spectrum that occurs with increased temperature is a decrease in CD_{231} (Figure 2A, inset). Changes in the CD spectrum between 200 and 220 nm are small, indicating that the secondary structure of Hx remains largely unaffected at even the highest temperatures we have studied so that the changes in ultraviolet absorbance and CD_{231} must reflect primarily changes in tertiary structure. For this reason, we refer to the process responsible for the large, thermally induced spectroscopic transitions described below as reorganization rather than denaturation.

The thermally induced change in CD_{231} that occurs with reorganization of Hx in sodium phosphate buffer (Figure 2B and Table 1) exhibits a midpoint transition temperature, T_m, of 44.8 ± 0.2 °C. Similar analysis of the average Tyr exposure to solvent, *r*, determined from second derivative spectra, yielded a T_m of 45.3 ± 0.7 °C (Figure 3A and Table 1). The excellent agreement between these values indicates that under these conditions, the changes in Tyr exposure occur in tandem with disruption of the tertiary structure of Hx. Furthermore, high concentrations of NaCl (e.g., ~140 mM in PBS) exert a significant stabilizing influence on Hx structure as indicated by both CD_{231} and the overall exposure of Tyr residues (Figures 2B and 3A, respectively). For human Hx, the T_m of Hx in PBS is at least 15.4 °C higher than that observed in 10 mM phosphate buffer alone (Table 1).

Influence of Metal Ions on Thermal Reorganization of Hx Structure As Assessed by Near-UV CD. The effect of metal ions on the temperature-induced change in CD_{231} for Hx in sodium phosphate buffer (Figure 2B, Table 1) indicates that Mn^{2+} has no detectable effect on the T_m of Hx while Ni^{2+}, Zn^{2+}, and Cu^{2+} reduce the T_m of the protein by as much as 4.8 °C. Binding of Co^{2+}, on the other hand, increases the T_m of the protein marginally (~0.6 °C). The control sample containing a chloride concentration equivalent to that contributed by the metal salts in these studies (200 μM NaCl) exhibited a T_m that was within the error of that observed for Hx in buffer alone.

In addition to altering the T_m of Hx (Table 1), various metal ions exhibit significant differences in the manner in which they influence the change in CD_{231} immediately before the transition (Figure 2A). This parameter, m_f (defined in eq 1 of ref *16*), represents the linear temperature dependence of the ellipticity of the folded structure, and binding of metal ions makes this parameter increasingly negative in the order $Zn^{2+} \sim Mn^{2+} \ll$ NaCl $\sim Cu^{2+} <$ buffer only $< Ni^{2+} \sim Co^{2+}$ (10 mM phosphate buffer, pH 7.4). In addition, the portion of the melting curve between 3 and 10 °C exhibits some curvature (i.e., steeper negative slopes toward lower temperatures) with addition of Mn^{2+} or Cu^{2+} (data not shown), suggesting that alternative low-temperature structure(s) comprise the native state of these Hx−metal ion complexes.

In contrast, effects of metal ions on the temperature dependence of the ellipticity of the reorganized structure (i.e., above the T_m) are much less pronounced than that observed for the native structure (Figure 2A). Various metal ions exhibit inequivalent effects on the slope of the posttransition ellipticity as reflected by the parameter m_u (eq 1, ref *16*). Of the metal ions examined, Cu^{2+} had the greatest effect on m_u, with m_u becoming more negative in the order $Cu^{2+} \ll Co^{2+} \sim Ni^{2+} \sim Zn^{2+} <$ NaCl $\sim Mn^{2+} \sim$ buffer only. Above 85 °C, the change in CD_{231} (Figure 2A) begins to flatten or turns slightly upward. This behavior at very high temperature is correlated with the observation that samples that were thermally reorganized at pH 7.4 contain small amounts of high molecular weight material [>130000 MW by SDS−PAGE run in the presence of DTT (data not shown)]. At pH 5.0, incubation of Hx samples at temperatures >85 °C for comparable periods of time does not result in formation of these large oligomers. On the basis of this pH effect, it seems likely that succinimide formation (*30*, *31*) and the subsequent

Table 1: Spectroscopically Determined Thermodynamic Parameters for Thermal Reorganization of Human Hx and Hx−Heme Complexes Formed with Metal Ions[a]

	technique						
	Hx						
	ellipticity (231 nm)				Tyr exposure[b]	Hx−heme[d]	
sample	T_m (°C)	ΔH_m (kcal/mol)	m_f (mdeg/°C)	m_u (mdeg/°C)	T_m (°C)	T_m (°C)	ΔH_m (kcal/mol)
sodium phosphate buffer (10 mM, pH 7.4)							
Hx−heme						64.6	105
Hx	44.8	78	−0.037	−0.088	45.3		
+200 μM NaCl	45.0	60	−0.031	−0.078	46.2		
+100 μM Mn^{2+} [c]	45.0	70	−0.016	−0.082	47.3	64.4	107
+100 μM Co^{2+}	45.6	47	−0.043	−0.068	45.8	63.1	111
+100 μM Ni^{2+}	43.0	39	−0.041	−0.073	41.8	61.0	102
+100 μM Zn^{2+}	40.8	55	−0.010	−0.073	42.6	58.1	90
+100 μM Cu^{2+} [c]	40.0	35	−0.031	−0.053	40.0	59.8	66
PBS							
Hx−heme						72.5	182
Hx	60.2	107			61.2		
+100 μM Zn^{2+}	59.6	105			60.2	70.9	140

[a] [Hx] = 5 μM in all cases. On the basis of reproducibility of replicate thermal reorganization data sets, the errors for CD_{231} data are estimated to be ±0.2 °C for T_m, ±2 kcal/mol for ΔH_m, ±0.003 mdeg/°C for m_f and m_u, and ±0.7 °C for T_m derived from Tyr exposure calculations. [b] From second derivative spectra (*27*). [c] Only data obtained at >7 °C were used in calculation of thermodynamic parameters. [d] Data from Rosell et al. (*16*). In this work thermodynamic parameters for heme release from Hx−heme were determined by monitoring changes in the Soret absorbance. The error in these values is estimated to be ±0.3 °C for T_m and ±5 kcal/mol for ΔH_m.

cross-linking reactions that occur with a pH optimum between pH 7 and 8 (*32*) are responsible for the production of these high molecular weight products and related ellipticity changes observed at very high temperatures although Trp-mediated disulfide bond cleavage and associated cross-linking reactions (*33*) may also contribute. In contrast, SDS−PAGE shows extensive cleavage of samples thermally reorganized in the presence of Cu^{2+}, a finding that is not surprising inasmuch as Cu^{2+} is known to catalyze peptide bond hydrolysis by means of a variety of possible oxidative mechanisms (*34*−*36*). Peptide bond cleavage resulting in some loss of secondary structure would explain the shallower posttransition slope observed for the Hx−Cu^{2+} complex.

Influence of Metal Ions on Thermal Reorganization of Hx Structure As Assessed by Average Tyr Exposure to Solvent. Analysis of absorption spectra by the method of Ragone et al. (*27*−*29*) provides a measure, indicated by the parameter *r*, of the extent to which Tyr residues are exposed to solvent. For human Hx, the presence of 16 tyrosyl residues precludes discrimination of behavior of individual residues, so *r* reflects the average solvent accessibility of Tyr residues. The thermal dependence of *r* exhibits many similarities to the thermal dependence of CD_{231} (Figures 2B and 3A). However, in the presence of Mn^{2+}, the two methods yield different results, with the T_m for change in Tyr exposure occurring 2.3 °C higher than the T_m observed for CD_{231}. In both methods of analysis, Cu^{2+} is the most destabilizing (T_m = 40.0 °C) of the metal ions examined. Both Ni^{2+} and Zn^{2+} decrease T_m, but the relative magnitude of their observed effect on Hx is slightly technique dependent (Table 1).

Influence of Metal Ions on Hx Structure As Assessed by Average Trp Exposure to Solvent. To gain insight into the basis for metal ion-induced changes in T_m observed in thermal reorganization experiments, the method of Shevchenko et al. (*26*) was used to measure the effect of metal ions on the Trp exposure at 20 °C. This analysis indicates that Cu^{2+}, Zn^{2+}, and Ni^{2+} increase the degree of tryptophan shielding (i.e., decrease tryptophan solvent accessibility) in Hx (Figure 3B). The magnitudes of these changes are not large, perhaps reflecting the overall stability of the protein structure attributable to the six disulfide bonds in the sequence. Indeed, even in the presence of 6 M GdnHCl (20 °C), the protein exhibits a 50.4% shielding of tryptophan from solvent. The CD spectrum in the presence of 6 M GdnHCl (Figure 2A, inset) confirms retention of significant β-sheet structure (*37*).

Thermally Induced Difference Absorption Mapping (TIDAM) in Assessment of Metal Ion-Linked Thermal Structural Reorganization of Human Hx. Thermal perturbation difference spectroscopy (*22*, *38*−*40*) has been used to estimate the number of aromatic residues at protein surfaces and in fluid environments under conditions that no conformational changes occur. In these earlier studies, ultraviolet spectra were collected at 10−15 °C intervals, and the temperature dependences of molar absorptivities were compared with those of individual amino acids. In the present work, we have modified this approach to study small changes in protein conformation induced by the binding of metal ions. In these experiments, incremental temperature changes (ΔT = 2.5 °C) are applied over a broad temperature range to assess thermally induced changes in the ultraviolet spectrum of Hx that result from structural rearrangements. Comparison of the contour plots of thermally dependent ultraviolet absorption spectra obtained in the presence and absence of metal ions permits observation of subtle changes in thermal structural perturbations that result from binding of metal ions. Analysis of such data by a method we refer to as thermally induced difference absorption mapping (TIDAM) affords enhanced visualization of spectroscopic changes arising from conformational dynamics.

The changes observed by TIDAM with Hx in PBS (10−90 °C) are shown in Figure 4. The areas designated as A through F on the right panel denote regions that are either common to all our experiments or that are affected by the presence of metal ions. The difference spectra in area A (10−15 °C, 260−290 nm) comprise a less intense version of the

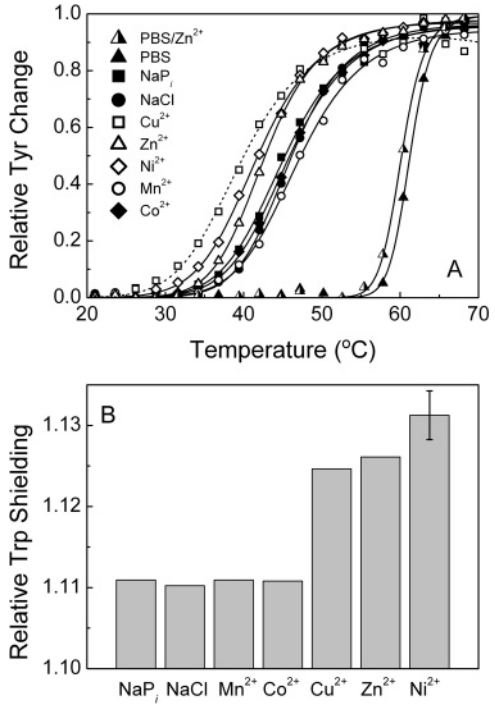

FIGURE 3: Solvent accessibility of aromatic residues in Hx and Hx−metal ion complexes. (A) Thermal dependence of changes in tyrosine exposure determined from second derivative UV absorption spectra by the method of Ragone (*27*). The effect of metal ions on Hx (5 μM) was examined in sodium phosphate buffer (10 mM, pH 7.4) (■), supplemented with 100 μM $CuCl_2$ (□, dotted line), $NiCl_2$ (◇), $ZnCl_2$ (△), $CoCl_2$ (◆), $MnCl_2$ (○), or 200 μM NaCl (●), and in PBS (▲) with 100 μM $ZnCl_2$ (▲). The lines are constructed from the fit parameters determined for eqs 1−3 of ref *16*. (B) Effect of metal ions on the tryptophan shielding determined according to the method of Shevchenko et al. (*26*). Measurements were made at 20 °C in sodium phosphate buffer (10 mM, pH 7.4) with a metal ion concentration of 100 μM or a sodium chloride concentration of 200 μM. Changes are relative to measurement of tryptophan shielding in 6 M GdnHCl. Values >1 indicate an increase in tryptophan shielding from solvent over that observed in 6 M GdnHCl. The maximum error, represented by the bar, is shown for Ni^{2+}.

spectrum of native Hx (Figure 4, left panel, and Figure 1A), consistent with decreasing absorptivities of tyrosyl and tryptophanyl residues with increasing temperature as part of a dipolar effect. A disproportionate absorbance change in the 290 nm region relative to 280 nm (e.g., area D), on the other hand, is consistent with the blue shift in the absorbance maximum and decreased intensity that generally results from transfer of Tyr or Trp to a more polar environment (*25*, *41*−*44*).

Area B (15−35 °C) is highly dependent on solution composition and in many cases exhibits sharp intensity fluctuations that are attributable to substantial structural changes of the protein. In sodium phosphate buffer (10 mM, pH 7.4), changes in this area are particularly prominent in the presence of Mn^{2+} or Zn^{2+} (Figure 5), but this effect is eliminated by the addition of EDTA. For example, addition of 200 μM EDTA (pH 7.4) to a 5 μM Hx solution containing 100 μM $MnCl_2$ followed by thermal reorganization results in a TIDAM profile that is virtually indistinguishable from that of Hx in sodium phosphate buffer (Figure 5). A strong inverse correlation can be observed between the intensity fluctuations in areas A and B (Figures 4 and 5) and the slope m_f in the CD_{231} profiles preceding reorganization (Figure 2A and Table 1). The larger the absorbance fluctuation in areas A and B (e.g., Mn^{2+}, Zn^{2+}), the smaller the change in CD_{231} signal with increasing temperature in the premelt region (i.e., the flatter the baseline that precedes the reorganization or the closer $m_f \rightarrow 0$). Thus, binding of these metal ions to Hx influences the distribution of conformations that the protein populates prior to the principal thermally induced reorganizational transition.

The structural dynamics reflected by areas A and B (Figure 4) are distinct from the thermal processes related to areas C, D, and E, which occur in the temperature range of the principal reorganizational transition. On the basis of the wavelength position (~260−265 nm) and band shape, area C includes a significant contribution from an increase in the number of solvent-exposed phenylalanyl residues (*22*) as reorganization proceeds. The number of such residues that contribute to this spectroscopic feature cannot be determined, however. Area D (~291 nm) can be ascribed to a change in the microenvironment(s) of one or more tyrosyl residues, while area E (~295 nm) primarily reflects changes in the tryptophan environment.

Overall, the positions of areas C, D, and E relative to the T_m (Figures 4 and 5, dashed line) along the temperature axis permit visualization of the course of structural reorganization that is linked to temperature and binding of metal ions. Under most conditions, areas C and D are isothermal. A notable exception is the case of the Hx−Mn^{2+} complex for which area C reaches a minimum ~8 °C before area D reaches a maximum (Figure 5). This finding correlates well with the T_m measurements in which the T_m from the CD_{231} is 2.5 °C lower than that obtained by monitoring tyrosine exposure. These observations suggest that, in the presence of Mn^{2+}, significant conformational changes involving average tyrosine exposure occur late in the reorganization process. An increase in tyrosine environment polarity is also shown by the characteristic blue shift in the spectrum (Figure 6B).

Area E represents the late stages of structural reorganization. The negative intensity change characteristic of this area may arise from increased conformational flexibility as reorganization nears completion, and an increase in interaction between tryptophan residues becomes possible. An alternative explanation for this spectroscopic result may be an increase in tryptophan shielding as the result of aggregation of Hx. Upon completion of the principal reorganization transition, the thermal profiles are relatively featureless [e.g., area F (Figure 4)], resembling to some extent the thermal profile of Hx in GdnHCl (Figure 5). Consequently, spectroscopic changes represented by area F result from thermal perturbation of surface residues.

DISCUSSION

Spectroscopic assessment of protein structure for the circulating form of plasma Hx is more challenging than for the Hx−heme complex because the circulating form lacks the heme group as a spectroscopically sensitive reporter. For this reason, we have studied the ultraviolet absorption and CD spectra of the protein to characterize the changes in Hx structure that accompany thermal reorganization and the influence of metal ion binding on these changes. In the CD spectrum, spectroscopic contributions of the secondary structure (e.g., negative Cotton effect at 222 nm) overlap

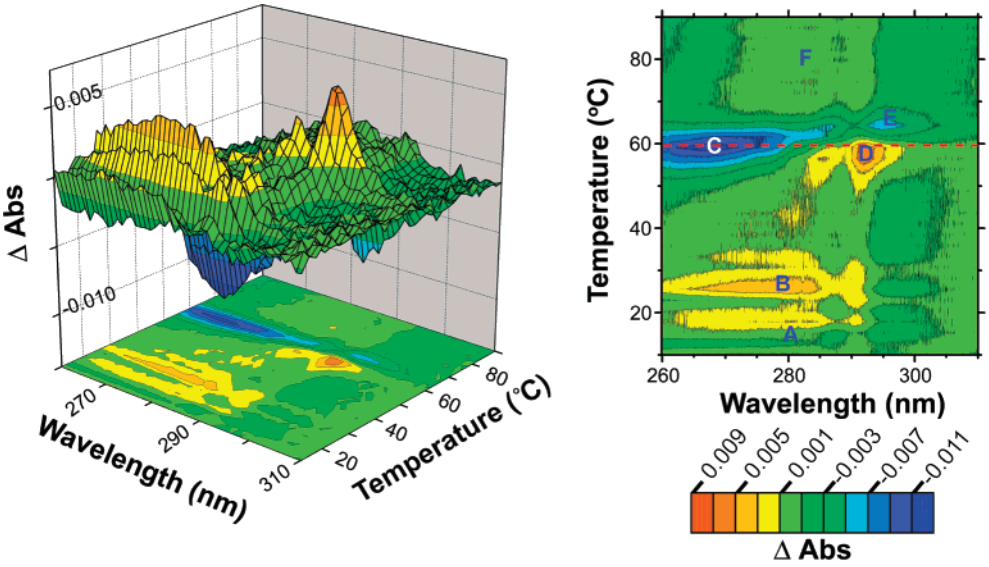

FIGURE 4: Examination of structural dynamics of Hx by thermally induced difference absorption mapping. The panel on the left provides the thermally induced difference spectroscopic surface of Hx (5 μM) in PBS constructed from UV absorbance spectra using sequential 2.5 °C perturbations. This surface is presented as a contour plot in the panel on the right. Boundaries between absorbance change intervals are indicated by black lines. The dashed line is the T_m for the thermal transition monitored by CD at 231 nm. The areas indicated by letters identify spectroscopic features discussed in the Results section.

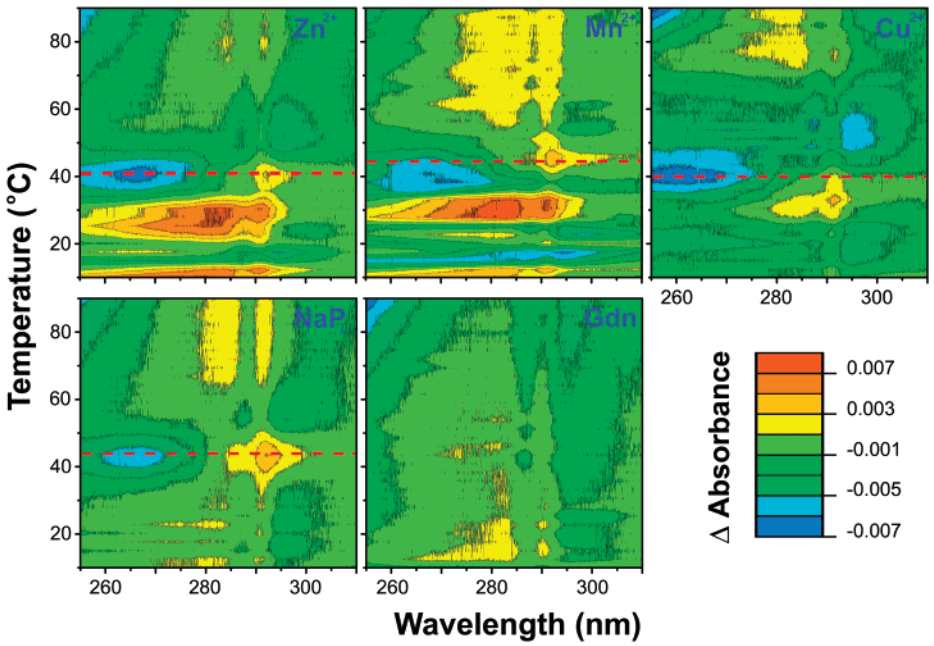

FIGURE 5: Examination of the effect of metal ions and GdnHCl on the structural dynamics of Hx by thermally induced difference absorption mapping. UV absorbance thermal perturbation difference contour maps are shown for Hx [5 μM protein in sodium phosphate buffer (10 mM, pH 7.4)] in the presence of 100 μM Zn^{2+}, Mn^{2+}, or Cu^{2+} or 6 M GdnHCl. The dashed lines on the contour plots are the T_m determined by monitoring CD_{231}.

those of the tertiary structure that are attributed to through-space interactions of Trp residues (positive Cotton effect ~230 nm) (*45*). For rabbit Hx, this positive ellipticity originates entirely from the C-domain and probably involves Trp256 and Trp268 (*13*, *19*, *46*). Presumably, corresponding features in the spectrum of the human protein are responsible for this marker band of tertiary structure. In the UV absorption spectrum, intensity variations associated with the change in microenvironment of a few aromatic residues are small relative to the total absorption of the aromatic residues of human Hx (19 Phe, 16 Tyr, 18 Trp). We have, therefore, used changes in CD_{231} and derivative electronic absorption spectroscopy to examine the effect of metal ion binding on thermal stability and the related structural dynamics of human Hx.

The characteristic shape of the Hx derivative absorption spectrum is produced by the interference pattern of the component aromatic absorption bands (*22*). The complex changes in these derivative spectra that occur with increasing temperature result from changes in environments of aromatic residues that affect both absorption intensity and wavelength maxima [e.g., increased polarity in the environment of aromatic residues results in blue shifts in the bands (*25*)] coupled with the intrinsic temperature-dependent changes to the absorbances of individual residues [e.g., tyrosine undergoes a red shift of ~0.9 nm over the temperature range of

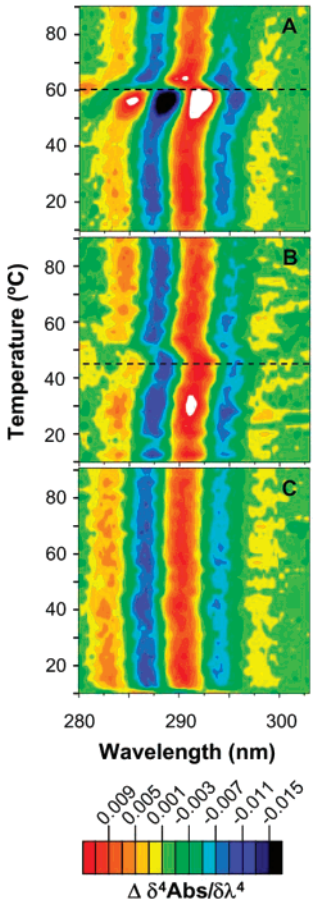

FIGURE 6: Influence of temperature on the structure of Hx as detected by thermally induced difference absorption maps constructed from fourth derivative absorption spectra. The contour plots are shown for 5 μM Hx in (A) PBS, (B) sodium phosphate buffer (10 mM, pH 7.4) with Mn^{2+} (100 μM), and (C) sodium phosphate buffer (10 mM, pH 7.4) with 6 M GdnHCl. T_m values determined from the thermal dependence of CD_{231} are shown by the dashed lines.

our experiments (*47*, *48*)]. Nevertheless, selected ratios of absorbance derivative intensities (*27*, *28*) allow specific monitoring of tyrosine exposure. Consequently, we can examine the effects of metal ions on individual types of aromatic amino acid residues.

Effects of Salt on Stability of Hx. Unlike some proteins (e.g., ref *49*), Hx demonstrates a substantial increase in thermal stability in the presence of sodium chloride (*16*, *50*, *51*). For human Hx in sodium phosphate buffer (10 mM, pH 7.4), the addition of 140 mM NaCl increases the T_m as detected by the change in CD_{231} by 15.4 °C (Table 1). This stabilizing effect is comparable to that produced by the addition of heme ($\Delta T_m = +16.0$ °C; cf. Table 1 of ref *16*). Coordination of heme iron to axial ligands His213 (in the flexible linker region) and His270 (in the C-domain) and formation of salt bridges involving the heme propionate groups and several basic residues in both domains are expected to stabilize the tertiary structure of the protein considerably. The stabilizing effect of NaCl may be due to ion binding within the central tunnels of the β-propeller structure of each domain [as observed in the crystal structure of rabbit Hx (*13*, *52*)] as well as to more general electrostatic interactions in the linker region or at the acidic patches at the entrance to the tunnels that are comprised of Asp286, Asp338, and Asp381 [in site J (*14*)] and Asp34, Glu50, Asp75, and Asp121 [site K (*14*)] in the model of the human Hx structure (Figure 7). Anions other than chloride have been shown previously to stabilize the Hx−heme complex (*16*). The destabilizing effect of certain metal ions (e.g., Zn^{2+}) persists but to a lesser degree in the presence of high levels of sodium chloride (Table 1, present work, and ref *16*).

Effects of Metal Ions on Stability of Hx. Of the metal ions used in our studies, Cu^{2+} destabilized Hx the most. Examination of the CD reorganization curves near the T_m and the related thermodynamic parameters (Figure 2B and Table 1) show that Hx has the lowest slope and ΔH_m in the presence of Cu^{2+}. Cu^{2+} also induced the lowest ΔH_m of the metal ions studied for the release of heme from Hx−heme (*16*). The reduced ΔH_m associated with the reorganization of Hx in the presence of Cu^{2+} presumably results from occurrence of structural forms intermediate between the folded and unfolded states of the protein (*16*, *53*). Such species could arise from partial stabilization of normally transient intermediates through binding of Cu^{2+}.

The next lowest ΔH_m obtained from CD_{231} measurements resulted from binding of Ni^{2+} to Hx (Table 1). Previous NMR studies of Ni^{2+} binding to Hx at 25 and 37 °C (*17*) indicated

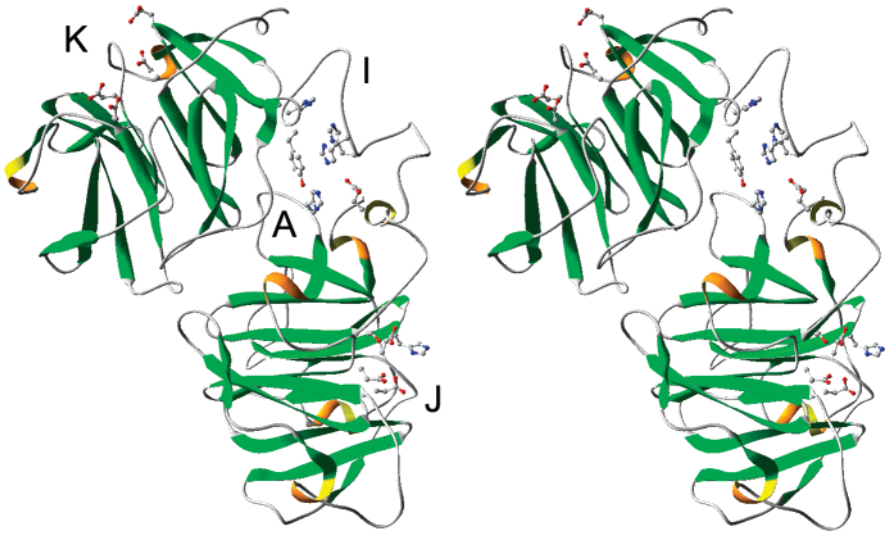

FIGURE 7: Stereo diagram of a structural model of human Hx (*14*) with the proposed binding sites for metal ions discussed in the text indicated.

that this metal ion binds at sites involving His that exhibit inequivalent temperature dependences. The combined results obtained with Ni^{2+} at present indicate that the presence of heme substantially reduces the heterogeneity of the available binding sites for Ni^{2+} but not for Cu^{2+}.

The binding of either Mn^{2+} and Zn^{2+} to Hx results in diminished temperature dependence of CD_{231} in the pretransition region of the thermal reorganization curves that provides evidence that the conformational flexibility evident in TIDAMs between 10 and 35 °C (Figure 5) is gained at the expense of chromophore mobility in the C-domain. Thus, an altered environment for the aromatic residues giving rise to the Cotton effect at 231 nm is induced upon binding of these metal ions to Hx. Interestingly, the m_f resulting from these aromatic groups with Mn^{2+} or Zn^{2+} bound to Hx approximates the m_f observed for the Hx−heme complex (*16*). An alternative explanation for the invariance in ellipticity over this temperature range requires a series of compensatory variations in dichroic strength to accompany the conformational dynamics of these Hx−metal ion complexes.

The Hx T_m value derived on the basis of tyrosine exposure calculations is elevated relative to the T_m from ellipticity at 231 nm in the presence of Mn^{2+} and to a less pronounced extent with Zn^{2+}. Because tyrosine residues in Hx are predominantly located in β-sheets [88% based on the crystal structure of rabbit Hx-heme (*13*)], the stability of these structural elements may be enhanced upon binding of these metal ions. The effects of alteration of surface charges on protein stability and conformation flexibility have been considered recently (*49*, *54*). Under the conditions of our experiments, the effects we see with Mn^{2+} should result from binding to a single, high-affinity site (*14*, *17*). Therefore, an alternative explanation for our T_m findings is that metal ion binding may increase the susceptibility of a single Tyr residue to dipolar effects and, thus, dominate the Tyr exposure profile. A likely candidate for this role is Tyr204, which is part of the putative metal ion binding site (Figure 7) proposed recently that involves Tyr204, His213, Glu230, and His270 [site A (*14*)]. This site includes both His residues that coordinate to the heme iron, so binding of metal ions to this site could be responsible for the m_f we observe. Binding of Zn^{2+} to the Hx−heme complex is proposed to occur near the linker region (*16*, *17*), possibly at a site involving His56 and His215 [site I (*14*)], thereby destabilizing the Hx−heme complex. Therefore, binding of Zn^{2+} to Hx could, in principle, occur at both of these adjacent sites and moderate the effects on Zn^{2+} on the spectroscopic properties of Tyr204.

Evaluation of protein conformational changes that occur in response to environmental factors solely through consideration of T_m values ignores more subtle structural changes that may be involved. To examine the response of Hx conformational dynamics to binding of metal ions, we have developed thermally induced difference absorption maps as a practical method that facilitates the analysis of small changes in protein tertiary structure by focusing on the global status of aromatic residues. Visualization of perturbations in electronic spectra that result from small structural changes by this analytical approach should be generally applicable to evaluation of structural dynamics of other proteins that remain soluble over a large range of temperature. In the current study, the conformational dynamics of Hx near physiological temperatures are shown to be affected substantially by metal ion binding. Consequently, binding ofmetal ions may modulate the heme scavenging properties of hemopexin in vivo.

REFERENCES

1. Tolosano, E., Hirsch, E., Patrucco, E., Camaschella, C., Navone, R., Silengo, L., and Altruda, F. (1999) Defective recovery and severe renal damage after acute hemolysis in hemopexin-deficient mice, *Blood 94*, 3906−3914.
2. Miller, Y. I., Smith, A., Morgan, W. T., and Shaklai, N. (1996) Role of hemopexin in protection of low-density lipoprotein against hemoglobin-induced oxidation, *Biochemistry 35*, 13112−13117.
3. Holt, S., Reeder, B., Wilson, M., Harvey, S., Morrow, J. D., Roberts, L. J., II, and Moore, K. (1999) Increased lipid peroxidation in patients with rhabdomyolysis, *Lancet 353*, 1241.
4. Morgan, W. T., and Smith, A. (2001) Binding and transport of iron-porphyrins by hemopexin, *Adv. Inorg. Chem. 51*, 205−241.
5. Delanghe, J. R., and Langlois, M. R. (2001) Hemopexin: a review of biological aspects and the role in laboratory medicine, *Clin. Chim. Acta 312*, 13−23.
6. Tolosano, E., and Altruda, F. (2002) Hemopexin: Structure, function, and regulation, *DNA Cell Biol. 21*, 297−306.
7. Smith, A., and Morgan, W. T. (1985) Hemopexin-mediated heme transport to the liver. Evidence for a heme-binding protein in liver plasma membranes, *J. Biol. Chem. 260*, 8325−8329.
8. Hvidberg, V., Maniecki, M. B., Jacobsen, C., Hojrup, P., Moller, H. J., and Moestrup, S. K. (2005) Identification of the receptor scavenging hemopexin-heme complexes, *Blood 106*, 2572−2579.
9. Herz, J., and Strickland, D. K. (2001) LRP: A multifunctional scavenger and signaling receptor, *J. Clin. Invest. 108*, 779−784.
10. Smith, A., Farooqui, S. M., and Morgan, W. T. (1991) The murine haemopexin receptor. Evidence that the haemopexin-binding site resides on a 20 kDa subunit and that receptor recycling is regulated by protein kinase C, *Biochem. J. 276*, 417−425.
11. Smith, A., and Hunt, R. C. (1990) Hemopexin joins transferrin as representative members of a distinct class of receptor-mediated endocytic transport systems, *Eur. J. Cell Biol. 53*, 234−245.
12. Baker, H. M., Norris, G. E., Morgan, W. T., Smith, A., and Baker, E. N. (1993) Crystallization of the C-terminal domain of rabbit serum hemopexin, *J. Mol. Biol. 229*, 251−252.
13. Paoli, M., Anderson, B. F., Baker, H. M., Morgan, W. T., Smith, A., and Baker, E. N. (1999) Crystal structure of hemopexin reveals a novel high-affinity heme site formed between two beta-propeller domains, *Nat. Struct. Biol. 6*, 926−931.
14. Mauk, M. R., Rosell, F. I., and Mauk, A. G. (2007) Structural modelling of metal ion binding to human haemopexin, *Nat. Prod. Rep. 24*, 523−532.
15. Takahashi, N., Takahashi, Y., and Putnam, F. W. (1984) Structure of human hemopexin: *O*-glycosyl and *N*-glycosyl sites and unusual clustering of tryptophan residues, *Proc. Natl. Acad. Sci. U.S.A. 81*, 2021−2025.
16. Rosell, F. I., Mauk, M. R., and Mauk, A. G. (2005) pH- and metal ion-linked stability of the hemopexin-heme complex, *Biochemistry 44*, 1872−1879.
17. Mauk, M. R., Rosell, F. I., Lelj-Garolla, B., Moore, G. R., and Mauk, A. G. (2005) Metal ion binding to human hemopexin, *Biochemistry 44*, 1864−1871.
18. Nozaki, Y. (1972) The preparation of guanidine hydrochloride, *Methods Enzymol. 26* (Part C), 43−50.
19. Wu, M. L., and Morgan, W. T. (1994) Conformational analysis of hemopexin by Fourier-transform infrared and circular dichroism spectroscopy, *Proteins 20*, 185−190.
20. Hider, R. C., Kupryszewski, G., Rekowski, P., and Lammek, B. (1988) Origin of the positive 225−230 nm circular dichroism band in proteins. Its application to conformational analysis, *Biophys. Chem. 31*, 45−51.
21. Morgan, W. T., and Muller-Eberhard, U. (1974) Modification of tryptophan residues of rabbit hemopexin by *N*-bromosuccinimide, *Enzyme 17*, 108−115.
22. Demchenko, A. P. (1986) *Ultraviolet Spectroscopy of Proteins*, pp 92−93, Springer-Verlag, New York.
23. Laue, T. M., Shah, B. D., Ridgeway, T. M., and Pelletier, S. L. (1992) Computer-aided interpretation of analytical sedimentation data for proteins, in *Analytical Ultracentrifugation in Biochemistry*

and Polymer Science (Harding, S. E., Row, A. J., and Horton, J. C., Eds.) pp 103−109, Royal Society of Chemistry, London.
24. Butler, W. L. (1979) Fourth derivative spectra, *Methods Enzymol. 56*, 501−515.
25. Lange, R., Frank, J., Saldana, J.-L., and Balny, C. (1996) Fourth derivative UV-spectroscopy of proteins under high pressure. I. Factors affecting the fourth derivative spectrum of the aromatic amino acids, *Eur. Biophys. J. 24*, 227−283.
26. Shevchenko, A. A., Kost, O. A., and Kazanskaia, N. F. (1994) Determination of solvent accessibility of residues of aromatic amino acids in proteins using the second derivative of the UV-absorption spectrum, *Biokhimiia 59*, 1707−1713.
27. Ragone, R., Colonna, G., Balestrieri, C., Servillo, L., and Irace, G. (1984) Determination of tyrosine exposure in proteins by second-derivative spectroscopy, *Biochemistry 23*, 1871−1875.
28. Havel, H. A. (1996) *Spectroscopic Methods for Determining Protein Structure in Solution*, VCH Publishers, New York.
29. Lange, R., and Balny, C. (2002) UV-visible derivative spectroscopy under high pressure, *Biochim. Biophys. Acta 1595*, 80−93.
30. Thannhauser, T. W., and Scheraga, H. A. (1985) Reversible blocking of half-cystine residues of proteins and an irreversible specific deamidation of asparagine-67 of *S*-sulforibonuclease under mild conditions, *Biochemistry 24*, 7681−7688.
31. Daniel, R. M., Dines, M., and Petach, H. H. (1996) The denaturation and degradation of stable enzymes at high temperatures, *Biochem. J. 317*, 1−11.
32. Aslam, M., and Dent, A. (1998) *Bioconjugation. Protein coupling techniques for the biomedical sciences*, pp 256, 381, Grove's Dictionaries, New York.
33. Vanhooren, A., De Vriendt, K., Devreese, B., Chedad, A., Sterling, A., Van Dael, H., Van Beeumen, J., and Hanssens, I. (2006) Selectivity of tryptophan residues in mediating photolysis of disulfide bridges in goat α-lactalbumin, *Biochemistry 45*, 2085−2093.
34. Rigo, A., Corazza, A., di Paolo, M. L., Rossetto, M., Ugolini, R., and Scarpa, M. (2004) Interaction of copper with cysteine: Stability of cuprous complexes and catalytic role of cupric ions in anaerobic thiol oxidation, *J. Inorg. Biochem. 98*, 1495−1501.
35. Kim, K., Rhee, S. G., and Stadtman, E. R. (1985) Nonenzymatic cleavage of proteins by reactive oxygen species generated by dithiothreitol and iron, *J. Biol. Chem. 260*, 15394−15397.
36. Allen, G. (2001) Specific protein degradation by copper(II) ions, in *Probing of Proteins by Metal Ions and Their Low-Molecular-Weight Complexes* (Sigel, H., Ed.) Vol. 38, pp 197−212, Marcel Dekker, New York.
37. Cantor, C. R., and Schimmel, P. R. (1980) *Biophysical Chemistry, Part II. Techniques for the study of biological structure and function*, p 427, W. H. Freeman, San Francisco.
38. Demchenko, A. P., and Zyma, V. L. (1975) Thermal perturbation spectroscopy of proteins. I. Medium polarity effects, *Stud. Biophys. 52*, 209−221.
39. Bello, J. (1969) The thermal perturbation method for the estimation of exposed tyrosines of proteins. I. Ribonuclease in aqueous glycol, glycerol, and denaturants, *Biochemistry 8*, 4542−4550.
40. Nicola, N. A., and Leach, S. J. (1976) Interpretation and applications of thermal difference spectra of proteins, *Int. J. Pept. Protein Res. 8*, 393−415.
41. Mach, H., and Middaugh, C. R. (1994) Simultaneous monitoring of the environment of tryptophan, tyrosine, and phenylalanine residues in proteins by near-ultraviolet second-derivative spectroscopy, *Anal. Biochem. 222*, 323−331.
42. Donovan, J. W. (1969) Changes in ultraviolet absorption produced by alteration of protein conformation, *J. Biol. Chem. 244*, 1961−1967.
43. Herskovits, T. T., and Laskowski, M., Jr. (1962) Location of chromophoric residues in proteins by solvent perturbation. I. Tyrosyls in serum albumins, *J. Biol. Chem. 237*, 2481−2492.
44. Marchal, S., Shehi, E., Harricane, M. C., Fusi, P., Heitz, F., Tortora, P., and Lange, R. (2003) Structural instability and fibrillar aggregation of non-expanded human ataxin-3 revealed under high pressure and temperature, *J. Biol. Chem. 278*, 31554−31563.
45. Kelly, S. M., and Price, N. C. (2000) The use of circular dichroism in the investigation of protein structure and function, *Curr. Protein Pept. Sci. 1*, 349−384.
46. Morgan, W. T., and Smith, A. (1984) Domain structure of rabbit hemopexin. Isolation and characterization of a heme-binding glycopeptide, *J. Biol. Chem. 259*, 12001−12006.
47. Chatani, E., Nonomura, K., Hayashi, R., Balny, C., and Lange, R. (2002) Comparison of heat- and pressure-induced unfolding of ribonuclease a: the critical role of Phe46 which appears to belong to a new hydrophobic chain-folding initiation site, *Biochemistry 41*, 4567−4574.
48. Mombelli, E., Afshar, M., Fusi, P., Mariani, M., Tortora, P., Connelly, J. P., and Lange, R. (1997) The role of phenylalanine 31 in maintaining the conformational stability of ribonuclease P2 from *Sulfolobus solfataricus* under extreme conditions of temperature and pressure, *Biochemistry 36*, 8733−8742.
49. Fayos, R., Pons, M., and Millet, O. (2005) On the origin of the thermostabilization of proteins induced by sodium phosphate, *J. Am. Chem. Soc. 127*, 9690−9691.
50. Wu, M. L., and Morgan, W. T. (1993) Characterization of hemopexin and its interaction with heme by differential scanning calorimetry and circular dichroism, *Biochemistry 32*, 7216−7222.
51. Shipulina, N. V., Smith, A., and Morgan, W. T. (2001) Effects of reduction and ligation of heme iron on the thermal stability of heme-hemopexin complexes, *J. Protein Chem. 20*, 145−154.
52. Faber, H. R., Groom, C. R., Baker, H. M., Morgan, W. T., Smith, A., and Baker, E. N. (1995) 1.8 Å crystal structure of the *C*-terminal domain of rabbit serum haemopexin, *Structure 3*, 551−559.
53. Hu, C. Q., and Sturtevant, J. M. (1987) Thermodynamic study of yeast phosphoglycerate kinase, *Biochemistry 26*, 178−182.
54. Strickler, S. S., Gribenko, A. V., Keiffer, T. R., Tomlinson, J., Reihle, T., Loladze, V. V., and Makhatadze, G. I. (2006) Protein stability and surface electrostatics: A charged relationship, *Biochemistry 45*, 2761−2766.

BI7008079